Environment International 142 (2020) 105814

Contents lists available at ScienceDirect

Environment International

journal homepage: www.elsevier.com/locate/envint

Black carbon dominates the aerosol absorption over the Indo-Gangetic Plain and the Himalayan foothills

S. Ramachandran[a,b,*], Maheswar Rupakheti[b], Mark G. Lawrence[b,c]

[a] Physical Research Laboratory, Ahmedabad, India
[b] Institute for Advanced Sustainability Studies, Potsdam, Germany
[c] Institute for Environmental Sciences and Geography, University of Potsdam, Potsdam, Germany

ARTICLE INFO

Handling Editor: Xavier Querol

Keywords:
Atmospheric aerosols
Characteristics
Absorption
Black carbon
Brown carbon
Dust
Himalayas
IGP
South Asia

ABSTRACT

This study, based on new and high quality in situ observations, quantifies for the first time, the individual contributions of light-absorbing aerosols (black carbon (BC), brown carbon (BrC) and dust) to aerosol absorption over the Indo-Gangetic Plain (IGP) and the Himalayan foothill region, a relatively poorly studied region with several sensitive ecosystems of global importance, as well as highly vulnerable populations. The annual and seasonal average single scattering albedo (SSA) over Kathmandu is the lowest of all the locations. The SSA over Kathmandu is < 0.89 during all seasons, which confirms the dominance of light-absorbing carbonaceous aerosols from local and regional sources over Kathmandu. It is observed here that the SSA decreases with increasing elevation, confirming the dominance of light absorbing carbonaceous aerosols at higher elevations. In contrast, the SSA over the IGP does not exhibit a pronounced spatial variation. BC dominates ($\geq 75\%$) the aerosol absorption over the IGP and the Himalayan foothills throughout the year. Higher BC concentration at elevated locations in the Himalayas leads to lower SSA at elevated locations in the Himalayas. The contribution of dust to aerosol absorption is higher throughout the year over the IGP than over the Himalayan foothills. The aerosol absorption over South Asia is very high, exceeding available observations over East Asia, and also exceeds previous model estimates. This quantification will be valuable as observational constraints to help improve regional simulations of climate change, impacts on the glaciers and the hydrological cycle, and will help to direct the focus towards BC as the main contributor to aerosol-induced warming in the region.

1. Introduction

Atmospheric warming is leading to an accelerated retreat of glaciers in the Himalayan-Tibetan Plateau region (Maurer et al., 2019). A major contributor to this warming is the absorption of sunlight by aerosol particles, especially black carbon (BC) and brown carbon (BrC), which are emitted from combustion sources, and natural dust particles, which dominantly contribute to the aerosol mass loading over many continental regions, including parts of the Indo-Gangetic Plain (IGP), the Himalayan foothills and the Tibetan Plateau (IPCC, 2013). However, quantitative determination and attribution of the atmospheric warming produced by these aerosol types has been difficult, especially due to a 50% uncertainty in their contribution to absorption aerosol optical depth (AAOD) (IPCC, 2013). Developing effective mitigation options for climate change over South Asia, a major aerosol hot spot, yet vulnerable and relatively poorly-studied region, requires a better quantification of the contributions of absorbing aerosol particles.

Though BC, BrC and mineral dust dominate the overall aerosol mass loading over South Asia (Jimenez et al., 2009), they exhibit a wide variability due to the large and regionally-varying sources and the monsoon seasonal dynamics (IPCC, 2013; Jimenez et al., 2009). BC and BrC are co-emitted during open biomass burning, domestic biomass combustion (cooking and heating), and fossil fuel combustion (Jimenez et al., 2009). Mineral dust from deserts and arid regions is transported to the Himalayan region from different origins by the summer and winter monsoon winds. BC is the strongest absorber per unit mass, with a single scattering albedo (SSA) of 0.19 compared to 0.85 for BrC and 0.84 for dust, but based on past measurements and model simulations it is a much smaller contributor to aerosol mass (5–10%) compared to BrC (16%) and dust particles (35%) over South Asia (Jimenez et al., 2009). Thus the BC contribution to total aerosol mass is 5–10 times less than the sum of BrC and dust, while the BC absorption (as 1-SSA) is over 5 times stronger than both BrC and dust, making it difficult to determine in advance what the relative contributions to aerosol absorption and

* Corresponding author at: Physical Research Laboratory, Ahmedabad, India.
E-mail addresses: ram@prl.res.in (S. Ramachandran), maheswar.rupakheti@iass-potsdam.de (M. Rupakheti), mark.lawrence@iass-potsdam.de (M.G. Lawrence).

https://doi.org/10.1016/j.envint.2020.105814
Received 9 January 2020; Received in revised form 15 April 2020; Accepted 9 May 2020

resultant atmospheric warming are. Global and regional models tend to significantly underestimate (by a factor of 2 to > 10) the observed BC mass concentrations in this region, as well as underestimating aerosol absorption in the southern Asian pollution outflow region (IPCC, 2013; Jimenez et al., 2009; Shindell et al., 2013; Menon et al., 2010). Modelling of BrC is even more difficult and uncertain than BC (Lawrence and Lelieveld, 2010). Model simulations of dust differ significantly in their sources (Textor et al., 2006) and long-range transport (Ramachandran et al., 2015), leading to large differences when compared to observations. The Atmospheric Chemistry and Climate Model Intercomparison Project (ACCMIP) which examined the short-lived drivers of climate change in current climate models found that models strongly underestimate absorbing aerosol optical depth (AAOD) in many regions; every model showed markedly less AAOD in South and East Asia (Shindell et al., 2013). In contrast to the available knowledge about the amount and type of aerosols in the outflow from East Asia to the Pacific, and from South Asia notably to the northern Indian Ocean, the Arabian Sea and the Bay of Bengal, much less is known about how much air pollution and which aerosol types make it to the Himalayan-Tibetan Plateau region, and the effects this has on the cryospheric reservoirs and the monsoon circulation (Lawrence and Lelieveld, 2010; Kang et al., 2019; Xu et al., 2016). Studies on surface measurements of BC, BrC and their contribution to total mass concentrations exist over the Himalayan-Tibetan Plateau region (e.g., Gustafsson et al., 2009; Li et al., 2016; Kang et al., 2019); however, studies of their contributions to the total column AOD have not been performed so far, although these would be very crucial for radiative forcing estimates and climate change assessments. The knowledge of the quantitative contribution of BC to aerosol absorption and to atmospheric warming is very important over this region because model simulations show that the high-altitude warming over the Tibetan Plateau and the Himalayan region due to BC could be as large as from CO_2 (~1.5 °C) (Xu et al., 2016). It should further be noted that it is rather difficult to measure AAOD accurately from space; for example, AAOD retrieved from the Ozone Monitoring Instrument (OMI) measurements have substantial biases (Shindell et al., 2013). In this context, for the first time, we analyze the spectral aerosol absorption characteristics from recently available high-quality ground-based observations over several locations in the Indo-Gangetic Plain (IGP) and the Himalayan foothills, providing observational constraints for the aerosol absorption due to BC, BrC and dust to the total column, and its significant environmental and climate implications over this aerosol hotspot region.

2. Study region

The Indo-Gangetic plain (IGP) (Fig. 1), covering parts of Pakistan, India, Bangladesh and Nepal, is a densely populated, intensely cultivated, industrialized and a heavily polluted region. Diverse aerosol emissions from natural and manmade sources (dust, BC, BrC, nitrate, sulfate and organics) give rise to a persistent blanket of haze characterized by a heavy aerosol loading over the IGP and downwind regions throughout most of the year (Lawrence and Lelieveld, 2010; Textor et al., 2006; Ramachandran et al., 2015). Studies conducted during the last decades documented the variations in aerosol characteristics and radiative forcing over this region (Lawrence and Lelieveld, 2010; Textor et al., 2006; Ramachandran et al., 2015), but were generally focused on a particular season and/or a particular location. We extend the focus of these observations by analyzing the measured columnar aerosol amount (in terms of aerosol optical depth (AOD)), and composition (in terms of AAOD and SSA) from several recently established AERONET (Holben et al., 2001) sites (https://aeronet.gsfc.nasa.gov/), providing a hitherto unavailable regional and temporal picture of the absorbing aerosol contribution over the IGP-Himalayan-Tibetan Plateau (HTP) region. The sites are located in the IGP and the central Himalayan foothills (Fig. 1). Lahore, New Delhi, Kanpur and Dhaka are urban, industrial and densely populated

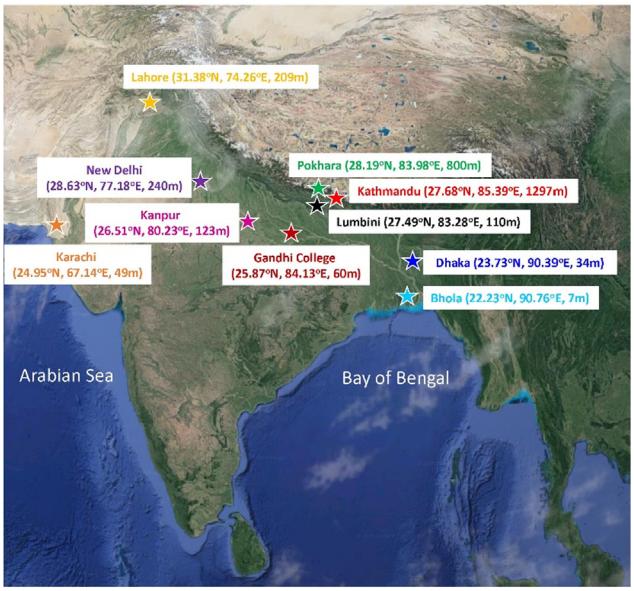

Fig. 1. Details of the study locations in the Indo-Gangetic Plain (IGP) and the Himalayan foothills in South Asia (the background map was generated with Google maps (https://www.google.com/maps). The latitude, longitude and elevation (in meters above sea level, m a.s.l.) of each location are given.

megacities (except Kanpur) with heavy air pollution. Kanpur is located ~ 500 km east of the megacity New Delhi. Karachi is a coastal megacity with two seaports. Gandhi College is a rural location in the central IGP. Bhola is the largest island of southern Bangladesh in the Bay of Bengal. The three sites in Nepal are located at increasing altitudes, from the northern edge of the IGP to the central Himalayan foothills with distinctly different environments in terms of geography and urbanization. Lumbini, the birthplace of the Buddha, is a rural area at the northern edge of the IGP, just before the altitude starts increasing towards the Himalayan mountains to the north. The Kathmandu Valley and Pokhara Valley are the largest and second largest metropolitan regions, both located in the Himalayan foothills, respectively, in Nepal. They are often downwind of the IGP. All the chosen study locations in this region are influenced by the South Asian monsoon system, with southwesterly winds during the summer monsoon and northeasterly winds during the winter monsoon, respectively (Lawrence and Lelieveld, 2010; Ramachandran et al., 2015).

3. Data and analysis

The level 2, version 3 cloud screened and quality assured daily data of aerosol optical depth (AOD), single scattering albedo (SSA), and absorption AOD (AAOD) were taken from measurements as part of the NASA Aerosol Robotic Network (AERONET) using ground-based CIMEL Sun/sky radiometers (Holben et al., 2001) which measure direct solar and diffuse sky radiances in the spectral range of 340–1020 nm for a period of a year over Lumbini (Jan-Aug 2013 and Sep-Dec 2017), Pokhara (Jan-Dec 2012) and Bode, Kathmandu (Jan-Mar, Jul-Dec 2013 and Apr-Jun 2014) (all in Nepal), and Karachi and Lahore (Pakistan) (Jan-Dec 2012), New Delhi (Jan-Dec 2009), Kanpur and Gandhi College (India) (Jan-Dec 2012), and Dhaka (Jan-Dec 2014) and Bhola (Jan-Dec 2015) (Bangladesh) (Table 1). As the objective is to cover one annual cycle over all the study locations, data sets were utilized corresponding to the years 2013–15, or 2012 when data were not available for 2013–2015. The years 2012–15 were chosen, since coincident data was available for almost all the months at most locations in this timeframe. Year round aerosol data for New Delhi were available only for 2009, which are utilized (Table 1).

Depending on the prevailing meteorological conditions over the

Table 1
Data availability at each station in each season. Number of days (daily averages) for which level 2, version 3, cloud screened and quality controlled aerosol properties data, available at each station during each season and their total, and utilized in the study.

Location	Winter	Pre-monsoon	Monsoon	Post-monsoon	Total
1. Lumbini	45	78	48	48	224
2. Pokhara	83	84	70	57	294
3. Kathmandu	81	76	59	41	267
4. Karachi	81	80	49	19	229
5. Lahore	58	82	107	56	303
6. New Delhi	31	46	48	14	139
7. Kanpur	54	72	63	29	218
8. Gandhi College	64	82	78	58	282
9. Dhaka	76	70	52	54	252
10. Bhola	81	80	37	48	246

IGP, analyzed data is classified into four seasons as winter (December-February), pre-monsoon (March-May), monsoon (June-September) and post-monsoon (October-November). Beyond the sites analyzed here, there are also two high altitude AERONET sites, at Nam Co (30.77°N, 90.96°E, 4746 m a.s.l.) on the Tibetan Plateau (China), and Ev-K^2-CNR (27.95°N, 86.82°E, 5079 m a.s.l.) near the base-camp of Mt. Everest (Nepal). No inversion data products (SSA, AAOD) are available for the Ev-K^2-CNR site. Furthermore, as the data from Nam Co are available only for a few days during 2012–15 (in Jan, Feb, May, Aug and Sep), we have not included the data from these locations in the study.

The uncertainty in AODs calculated using the direct solar radiation measurements is less than ± 0.01 for wavelengths > 440 nm and is less than ± 0.02 for shorter wavelengths (Holben et al., 2001). The error in SSA is ± 0.03 when the AOD at 440 nm is > 0.2 (Dubovik et al., 2000). The uncertainty in AAOD is ± 0.01 (Mallet et al., 2013). Aerosol properties corresponding to individual observations (made at 15–20 min time intervals), and typically about 20 daily measurements during the chosen year(s) are used to calculate the monthly and seasonal averages, and are utilized in the present work. We have used level 2, quality controlled, cloud screened and calibrated AERONET data in the study, and the uncertainties in these parameters are not expected to change any conclusions of the study. During the monsoon season over the study region, cloud screening reduces the number of data points used for analysis (Table 1). The AERONET retrieved aerosol properties have the highest accuracy for observations when solar zenith angle is between 50° and 80° (Dubovik et al., 2000), and only those data that are within this solar zenith angle range are utilized in the study.

The estimation of carbonaceous aerosol (CA) and dust AAOD (Chung et al., 2012a; Cho et al., 2019), and the subdivision into BC and BrC AAODs, was done utilizing monthly mean AAOD values at 440, 675 and 870 nm, calculated from daily average data. The spectral AAODs follow a power law of the form, $AAOD = K\,\lambda^{-AAE}$ where λ is the wavelength, and AAE is the Absorption Ångström Exponent. AAE is computed using AAOD values obtained at 440, 675 and 870 nm by least squares fitting of AAOD with respect to wavelength on a log–log plot. AAE_{Dust} and AAE_{CA} are assumed to be 2.4 and 1.16 (Chung et al., 2012a). The retrieved AAE_{Dust} value was 2.4 (which varied in the range of 2.2 to 2.6) (Chung et al., 2012a and references therein), and AAE_{CA} varies from 0.84 (North America, West Europe and East Asia) to 0.97 (eastern Europe) and 1.16 (South Asia) (Chung et al., 2012a). The value of 1.16, appropriate for South Asia, is used in this study. When the monthly mean AAE value calculated from the daily average values was < AAE_{CA}, or > AAE_{Dust}, then AAE was set to AAE_{CA} and AAE_{Dust}, respectively (Chung et al., 2012a). However, monthly mean AAE never exceeded 2.4 at the study locations in South Asia.

AAE_{Dust} and AAE_{CA} values were obtained from global observations of AERONET data (Chung et al., 2012a). AAE_{Dust} values were obtained from the AAE distribution when the α values were small (aerosols dominated by coarse mode particles (dust and sea salt)) (Chung et al., 2012a). As smaller α values can also occur due to the presence of sea salt mixed with polluted dust, and as dust can be internally mixed with BC, and as CA will have lower AAE values than pure dust, Chung et al. (2012a) adopted the 95th percentile of AAE values to represent pure dust. Following this procedure, AAE_{Dust} was derived to be 2.4, while the published values for AAE_{Dust} were in the range of 1.9 to 2.4 (Bergstrom et al., 2007; Eck et al., 2010; Russell et al., 2010), and the lower values of AAE_{Dust} were attributed to polluted dust (Chung et al., 2012a). AAE_{CA} values were obtained from the AERONET data in four regions – fossil fuel dominated areas (North America, West Europe and East Asia), Eastern Europe, South Asia, and biomass-burning dominated areas – from dust-free seasons and locations in these regions (Chung et al., 2012a).

The wavelength dependence of AOD and AAOD for dust and CA (BC, BrC) are significantly different (Chung et al., 2012a; Russell et al., 2010). Dust AOD is almost independent of wavelength in the 400–1000 nm wavelength region, while AOD for fossil fuel and biomass burning emissions exhibit a steep gradient with values at shorter wavelengths significantly higher than values at longer wavelengths (Chung et al., 2012a; Russell et al., 2010). In contrast, the absorption by dust increases steeply towards shorter wavelengths while the spectral CA absorption is less steep (Chung et al., 2012a). Among the carbonaceous aerosol species, light absorption due to BrC is strongly wavelength dependent (the absorption is significantly less than BC, effective only over a narrow wavelength band in the 300 to 600 nm wavelength range, and falls very sharply after 400 nm), it makes no significant contribution to total light absorption beyond 550 nm (< 5%), which was found to be smaller compared to global model estimates constrained by AERONET AOD observations (Kirillova et al., 2016). These different spectral features in dust, BC and BrC absorption effectively enables us to quantify the contribution of each absorbing species to AAOD. The contributions of CA and dust to the AAOD are distinguished using AAE, with the percentage contribution of CA to AAOD linearly decreasing and of dust linearly increasing with increasing AAE values (Fig. 2). CA and dust contribute equally (50%) when AAE is ~ 1.8.

A sensitivity analysis is performed to examine the effect of variations in the values of AAE_{CA} (=1.16) and AAE_{Dust} (=2.4). Cases 1 and 6 in Table 2 represent the percentage contributions of CA and dust aerosols to AAOD derived for two AAE values with AAE_{CA} = 1.16 and AAE_{Dust} = 2.4: case 1 with AAE = 1.35 and case 6 with AAE = 2.00. Cases 2 and 3 correspond to the percentage contributions of CA and dust aerosols with a 10% higher value of AAE_{CA} (case 2) and 10% lower value of AAE_{CA} (case 3) for AAE_{Dust} = 2.4. Cases 4 and 5 correspond to the percentage contributions of CA and dust aerosols with a 10% higher

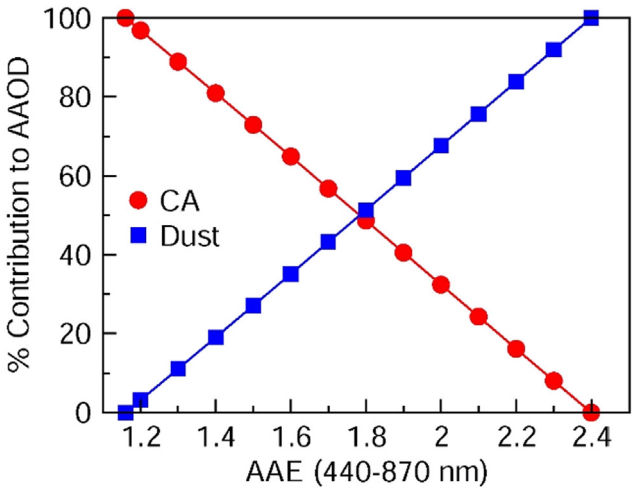

Fig. 2. Contributions of carbonaceous aerosol (CA) and dust to the absorption aerosol optical depth (AAOD) as a function of the Absorption Ångström Exponent (AAE).

Table 2
Sensitivity of AAE_{CA} and AAE_{Dust} to the percentage contribution of carbonaceous aerosol (CA) and dust to AAOD for an AAOD (at 550 nm wavelength) of 0.046 (rounded off to 2 decimal digits). AAE_{CA} and AAE_{Dust} are varied by 10% with respect to 1.16 and 2.4 respectively, and changes in the percentage contribution due to the variations in AAE_{CA} and AAE_{Dust} with respect to the percentage contribution due to CA and Dust to AAOD for AAE_{CA} of 1.16 and AAE_{Dust} of 2.4 are estimated.

Case	AAE	AAE		AAOD		% Contribution		Change in % contribution	
		CA	Dust	CA	Dust	CA	Dust	CA	Dust
1	1.35	1.16	2.40	0.039	0.007	84	16	–	–
2	1.35	1.28	2.40	0.043	0.003	93	07	9	−9
3	1.35	1.04	2.40	0.035	0.011	77	23	−7	7
4	1.35	1.16	2.64	0.040	0.006	87	13	3	−3
5	1.35	1.16	2.16	0.037	0.009	81	19	−3	3
6	2.00	1.16	2.40	0.015	0.031	33	67	–	–
7	2.00	1.28	2.40	0.016	0.030	36	64	3	−3
8	2.00	1.04	2.40	0.014	0.032	30	70	−3	3
9	2.00	1.16	2.64	0.020	0.026	44	56	11	−11
10	2.00	1.16	2.16	0.008	0.038	17	83	−16	16

value of AAE_{Dust} (case 4) and 10% lower value of AAE_{Dust} (case 5) for AAE_{CA} = 1.16. Results for the percentage contributions due to CA and dust aerosols for an AAE = 2.00 are shown in cases 7 to 10. The changes in the percentage contributions due to CA and dust aerosols are estimated with respect to the percentage contributions obtained for case 1 (AAE = 1.35) (for cases 2 to 5), and case 6 (AAE = 2.00) (for cases 7 to 10) respectively. The study reveals that the percentage change in CA and dust contributions differ between 3 and 16% (Table 2) for a 10% variation in the value of AAE_{Dust}, while they differ in the range of 3–9% for the case of a 10% variation in AAE_{CA}. The percentage change in CA and dust contributions are maximum when AAE_{CA} is increased by 10% (case 2) while it is maximum when AAE_{Dust} value is reduced by 10% (case 10) from their respective values of 1.16 and 2.4. The study shows that changes in the percentage contribution of CA and dust aerosols to AAOD also depend on the value of AAE with respect to the values of adopted AAE_{CA} (1.16) and AAE_{Dust} (2.4). It may be noted that the study by Chung et al. (2012a) relied more on observations compared to the earlier semi-empirical approaches (Chung et al., 2012a and references therein). The sensitivity analysis (Table 2) suggests that the uncertainty in the derived contributions of CA and dust aerosols to AAOD due to variations in AAE_{CA} and AAE_{Dust} values can be a maximum of 16% which compares well with the uncertainty estimates provided in Chung et al. (2012a).

The BC and BrC contributions to the AAOD of CA were estimated assuming AAE_{BC} and AAE_{BrC} to be 0.5 and 4.8, respectively (Chung et al., 2012a). AAE_{BC} was obtained from the lowest 10^{th} percentile of the fossil fuel aerosol AAE distribution which was 0.5; the AAE_{BC} values ranged between 0.38 and 0.67 (Chung et al., 2012a). It may be noted that published values of AAE_{BC} were in the 0.2 to 1.0 range; 0.2 was derived for thickly coated and transported BC (Chung et al., 2012b), and 1.0 was found to be near the pollution source (Kirchstetter et al., 2004). The published values of AAE_{BrC} vary widely from 3 to 6 (Sato et al., 2003; Kirchstetter et al., 2004). BC and BrC AODs are estimated using AAOD = AOD*(1-SSA), using the corresponding SSA values of 0.19 and 0.85 for BC and BrC, respectively (Chung et al., 2012a; Cho et al., 2019; Magi, 2011). The uncertainties in the SSA contribute to the uncertainty in BC and BrC AODs whereas the SSA for dust was obtained from the AERONET data used to generate AAE_{Dust} (Chung et al., 2012a).

4. Results and discussion

4.1. AAOD across the IGP and the Himalayas

The AAOD (=AOD*(1-SSA)) depends on the columnar content (AOD) and composition of aerosols (SSA) (Fig. 3). The AAOD depends more strongly on small differences in the SSA compared to the AOD (for example, for a typical AOD of 0.5 and composite SSA of a mixture of aerosol particles of 0.9, a 10% decrease in SSA leads to nearly a doubling of the AAOD, while a 10% increase in AOD leads to a 10% increase in AAOD); i.e., differences in aerosol composition generally more significantly influence the aerosol absorption than differences in aerosol column content. Among the sites in Nepal, the AAOD increases with increasing altitude, except in the post-monsoon season (Fig. 3a), during which Lumbini is affected by intense agro-residue burning emissions in the IGP leading to a higher AOD and lower SSA (Fig. 3a, b) (and thus a much higher AAOD (Fig. 3c, d)) than in other seasons. Kathmandu has the highest AAOD of all the locations during the pre-monsoon and monsoon seasons, while during the post-monsoon season the AAOD is highest over New Delhi and Dhaka, being strongly affected by agro-residue burning in this season (Jethva et al., 2018). SSA values exhibit notable differences (Fig. 3a, b), with SSA for Kathmandu being the lowest (0.82–0.89) among all the study locations throughout the year, except over New Delhi during the post-monsoon season (Fig. 3b) due to transport of aerosols emitted by regional biomass burning (Jethva et al., 2018). SSA values at the other locations are generally similar to each other, with monsoon values being a little higher than in the other seasons (Fig. 3b), and are in the range 0.89–0.96. Here we found that over all the sites in Nepal, the AAOD is governed mainly by SSA (i.e., composition or amount of absorbing aerosol loading), as anticipated based on the expected sensitivity considering the formula for calculating AAOD. In contrast, during the post-monsoon season, when SSA is comparable across the Nepalese sites, and throughout the year over the other locations, the AAOD is more influenced by AOD (i.e., amount of aerosol loading) than by differences in SSA.

Seasonal and annual mean AODs (Fig. 3a, b) are all > 0.3, indicating that all sites (except Kathmandu and Pokhara during both the monsoon and post-monsoon) are highly polluted (Ramanathan et al., 2007). During the pre-monsoon season, both agricultural and forest fires in the IGP and the Himalayan foothills, in addition to the regional transport of continental aerosols from polluted regions (Singh et al., 2019; Weissmann et al., 2005), lead to higher AODs over Pokhara and Kathmandu (elevated locations) (Singh et al., 2019; Mahapatra et al., 2019). During the monsoon, the regional transport of emissions such as from forest fires is suppressed due to monsoon rains, and further, some of the major seasonal sources, especially brick production, are less active in this season, resulting in lower AODs. Among the sites in the IGP, AODs increase from the west to the east during winter, while during the monsoon the AODs decrease from west to east. This spatial pattern in AODs during winter occurs due to the prevailing meteorological conditions (shallow atmospheric boundary layer and calm winds) being conducive to accumulating more aerosol mass, combined with increasing emissions towards the east (Lawrence and Lelieveld, 2010). The reduction in AODs is attributed to the progression and strength of the monsoon from the west to the east, with the relative reduction in AODs being more pronounced in Bhola and Dhaka than at the other locations, since they are close to the coast, and the greater amount of summer monsoon precipitation leads to a more substantial reduction in aerosol content through wet removal (Lawrence and Lelieveld, 2010) compared to the other IGP locations.

The annual and seasonal average SSA over Kathmandu is the lowest of all the locations. The SSA over Kathmandu is < 0.89 during all seasons, which confirms the dominance of light-absorbing carbonaceous aerosols from local and regional sources over Kathmandu, consistent with earlier results from surface and columnar observations for winter (Cho et al., 2017). The carbonaceous aerosols arise largely from

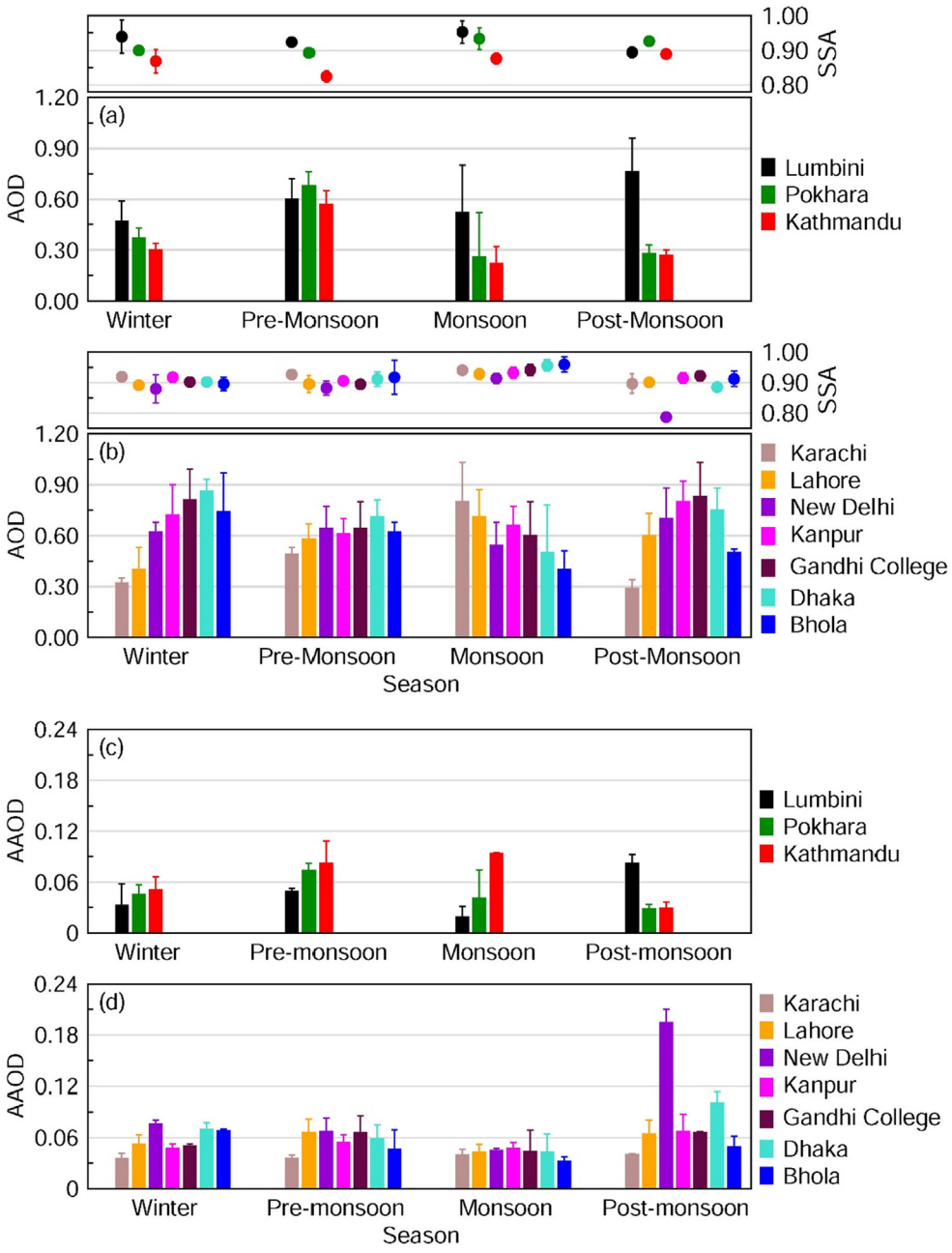

Fig. 3. Aerosol optical properties over the IGP and the Himalayan Foothills: (a, b) Seasonal mean aerosol optical depth (AOD) and single scattering albedo (SSA, overlying panels), (c, d) absorption aerosol optical depth (AAOD) corresponding to a wavelength of 550 nm. Vertical bars indicate ± 1σ (standard deviation) from the mean. The seasons are defined as winter: Dec-Feb, pre-monsoon: Mar-May, monsoon: Jun-Sep, and post-monsoon: Oct-Nov.

continental anthropogenic emissions (including from biomass burning) which get transported to higher elevations (Lawrence and Lelieveld, 2010; Singh et al., 2019). It is observed here that the SSA decreases with increasing elevation (Fig. 3a), confirming the dominance of light absorbing carbonaceous aerosols at higher elevations. In contrast, the SSA over the IGP does not exhibit a pronounced spatial variation, except over New Delhi during the post-monsoon season, when the SSA is lowest and the AAOD is highest among all the sites (Fig. 3b). This occurs as a result of the transport of smoke aerosol emissions from crop residue fires (Jethva et al., 2018), mixed with urban aerosols. The New Delhi site is impacted more by agro-residue burning during the post-monsoon season compared to the other IGP sites (Ramachandran et al., 2015). Even though AERONET data for the year 2009 is used for New Delhi in the current study (since this was the only year in the last decade with a full year of data available), satellite data showed that this is not an unusual year in terms of fire counts and AOD (Jethva et al., 2018).

4.2. Carbonaceous and dust aerosols

With regards to the attribution of the aerosol absorption to each aerosol type, we first analyzed the contributions of carbonaceous aerosol (CA) and dust, and found that CA dominates aerosol absorption across seasons and locations in the Himalayan foothills (Fig. 4). Based on the observed AAE values, CA contributes > 90% to AAOD in Lumbini and Kathmandu throughout the year, with the contribution over Kathmandu being maximum (computed to be 100%) during most of the year. Over Pokhara, CA contributes ~ 70% to the AAOD during the monsoon, and ~ 80% during the post-monsoon season. This is consistent with relatively higher values of SSA (> 0.93) observed over

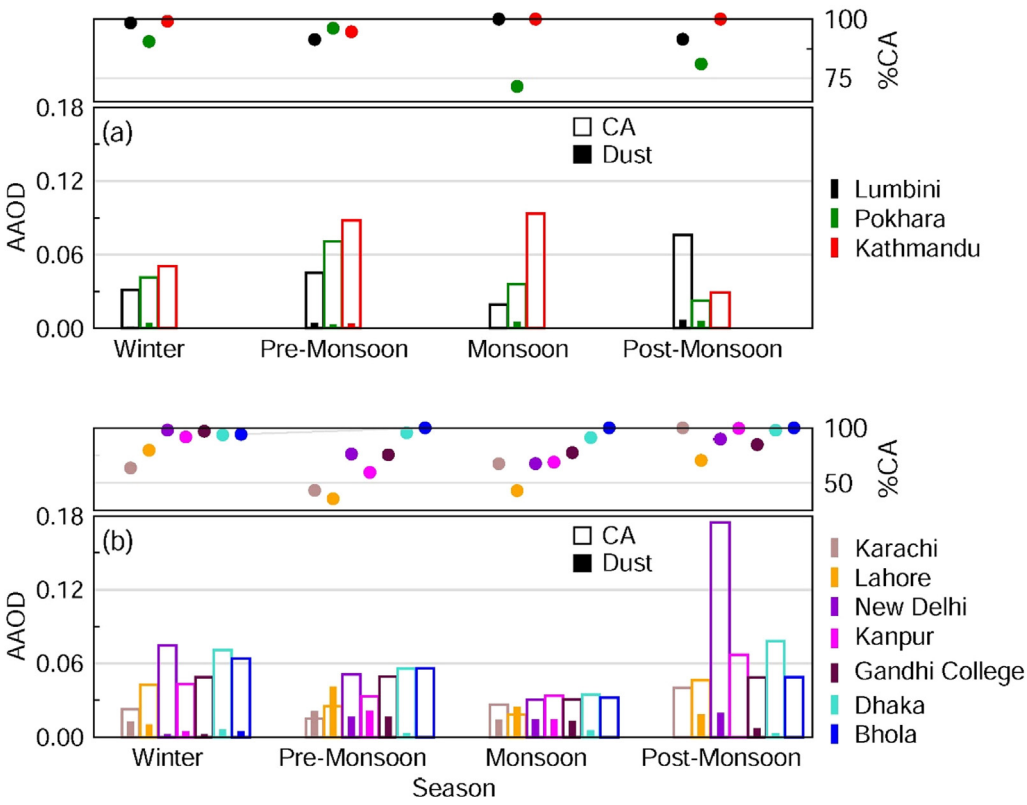

Fig. 4. Contributions of carbonaceous aerosol (CA) and dust to the absorption aerosol optical depth (AAOD) corresponding to a wavelength of 550 nm across seasons and locations in the IGP and Himalayan foothills: (a) Nepal locations and (b) other locations. The bottom panels show absolute contributions, while the overlying panels show the percentage of CA to the total.

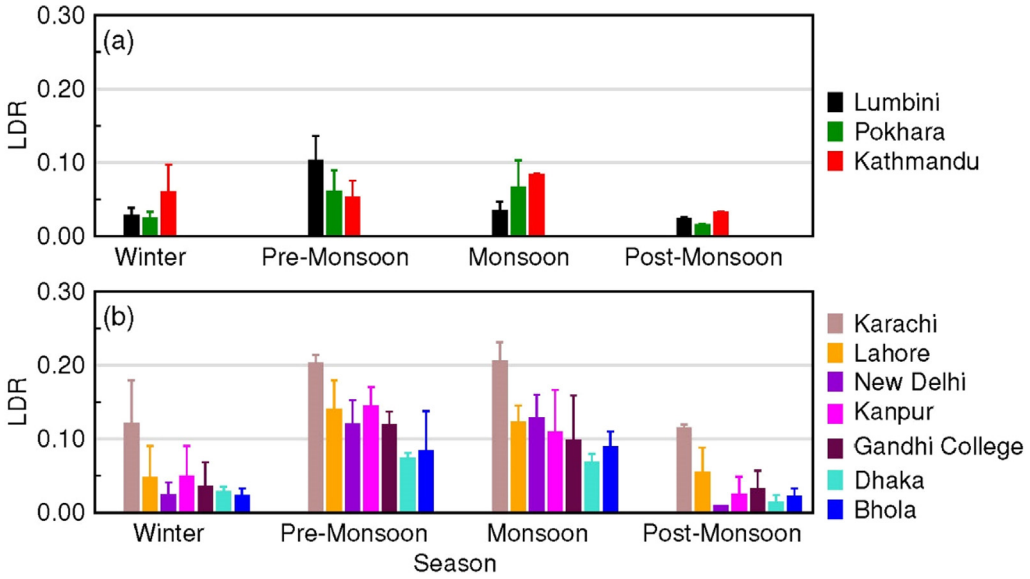

Fig. 5. Seasonal mean linear depolarization ratios (LDR) (at 532 nm) for all the locations in the IGP and Himalayan foothills. Vertical bars indicate ± 1σ standard deviation from the mean.

Pokhara during these seasons (Fig. 3). The SSA over Kathmandu, despite being located at a higher elevation, is lower than over both Lumbini and Pokhara. Vertical profile measurements over and around the Pokhara valley revealed that the BC concentration at elevated locations in the Himalayas was comparable to the surface (Singh et al., 2019), leading to lower SSA values (Fig. 3). CA contributes > 90% to AAOD over New Delhi, Kanpur, Gandhi College, Dhaka and Bhola during winter.

The contribution of dust to the AAOD is higher throughout the year over Karachi, Lahore, New Delhi, Kanpur and Gandhi College compared to Dhaka and Bhola (Fig. 4). During the pre-monsoon and monsoon, the contribution of dust over the IGP is greater due to transport of dust from arid and semi-arid regions, while the amount of dust decreases from west to east across the IGP, as observed in previous studies (Ramachandran et al., 2015).

Karachi has a higher SSA than Lahore as it is closer to the coast; sea salt particles are abundant near coast and effectively scatter radiation (SSA = 1.00), increasing the SSA of the total aerosol mix (Fig. 3). Similarly, the SSA over Gandhi College during the pre-monsoon season is lower when compared to Kanpur, due to the springtime increase in agro-residue burning surrounding Gandhi College (Ramachandran et al., 2015). We also examined the linear depolarization ratio (LDR),

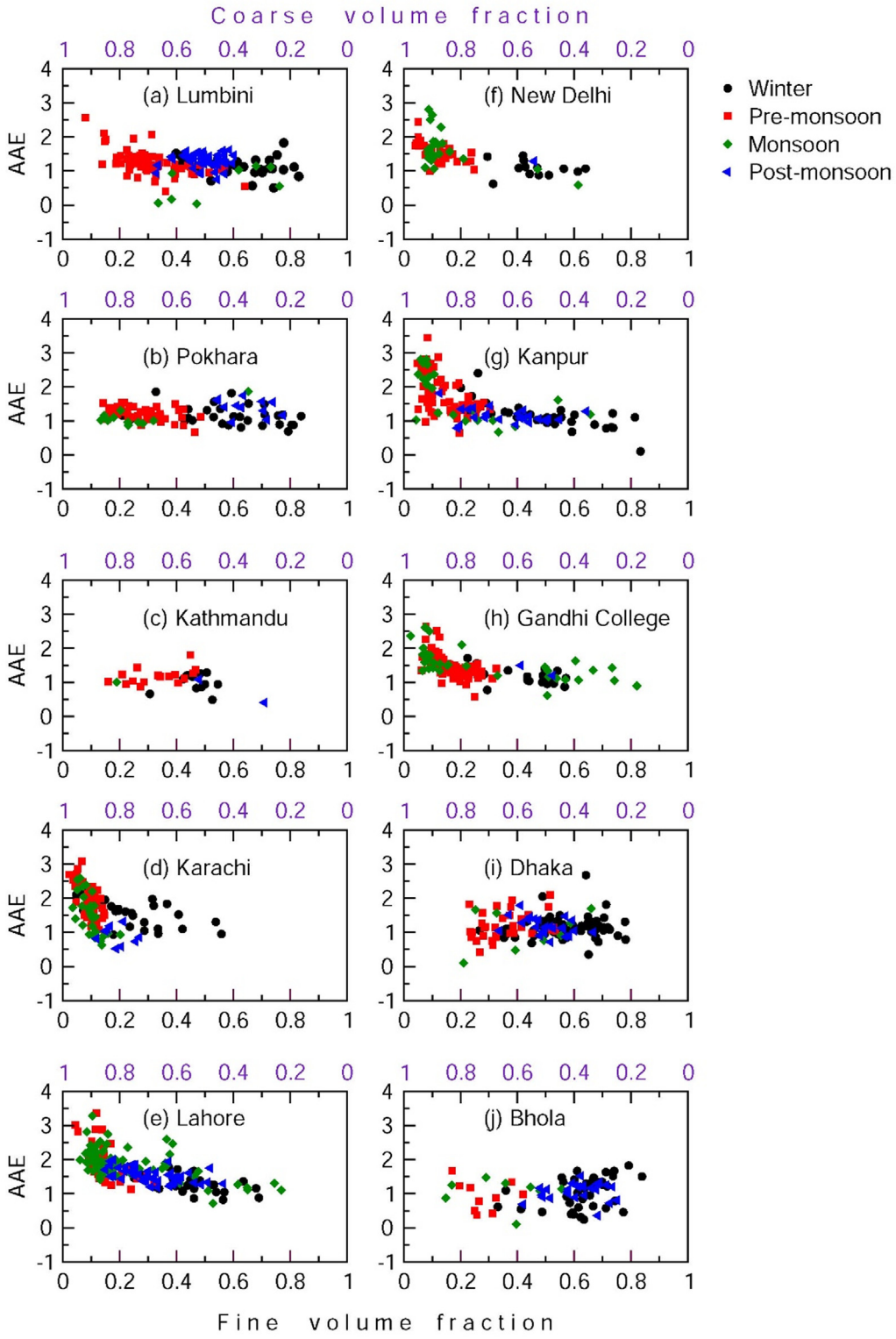

Fig. 6. Absorption Ångström Exponent (AAE) (derived using AAODs measured at 440, 675 and 870 nm) vs. fine and coarse volume fractions across seasons and locations in the IGP and Himalayan foothills: (a) Lumbini, (b) Pokhara, (c) Kathmandu, (d) Karachi, (e) Lahore, (f) New Delhi, (g) Kanpur, (h) Gandhi College, (i) Dhaka and (j) Bhola. Daily average values based on the available measurement dates are shown.

and found it to be ≥ 0.1 (Fig. 5) during the pre-monsoon season and the monsoon over Karachi, Lahore, New Delhi, Kanpur and Gandhi College, which is consistent with the increase in the amount of dust (coarse aspherical particles). In addition, the daily average fine volume fraction (fvf) (Fig. 6) is mostly < 20% during the pre-monsoon season and the monsoon over these five sites, confirming that coarse mode aerosols (mainly dust) dominate the aerosol volume fraction. In contrast, LDR ≤ 0.1, and fvf is ≥ 20% over the Himalayas, as well as over Dhaka and Bhola (Fig. 6) throughout the year, corroborating the dominance of fine mode aerosols emitted from urban/industrial sources and from biomass burning (Lawrence and Lelieveld, 2010; Ramachandran et al., 2015). It is interesting to note that the seasonal mean LDR is lowest

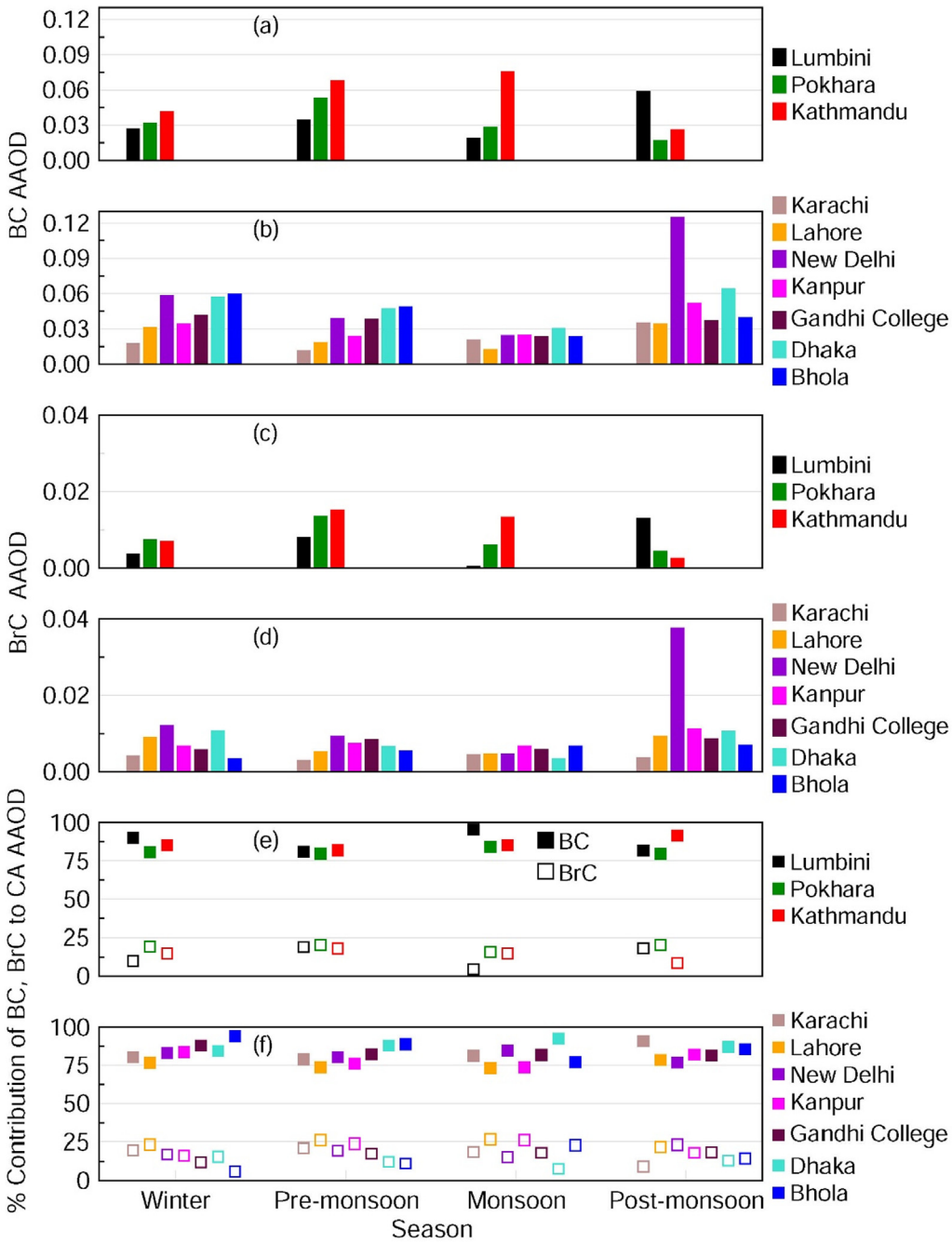

Fig. 7. Black carbon (BC) and brown carbon (BrC) over the IGP and the Himalayan Foothills: Seasonal mean values of: (a, b) BC AAOD, (c, d) BrC AAOD, and (e, f) percentage contribution of BC and BrC to CA AAOD corresponding to a wavelength of 550 nm. (For interpretation of the references to colour in this figure legend, the reader is referred to the web version of this article.)

over New Delhi during the post-monsoon season, confirming that the aerosols are spherical (having emanated from agro-residue fires in the surrounding regions and undergone intense atmospheric processing during transport (Jethva et al., 2018)).

4.3. Black carbon and brown carbon

When the contribution of CA to AAOD was split further into its two light-absorbing components, we found that BC dominates over BrC for the aerosol absorption over the IGP and the foothills of the Himalayas (Fig. 7). BC AAOD is highest in Kathmandu throughout the year, except during the post-monsoon, when it is highest over Lumbini (Fig. 7a). BC AAOD shows a gradual spatial increase from Karachi to Bhola (except for New Delhi) in the IGP during winter and the pre-monsoon season (Fig. 7b). The abundance of absorbing aerosols is higher during winter and the post-monsoon season over the IGP (Ramachandran et al., 2015), leading to higher AAODs. BC AAODs are low during the monsoon, and increase during the post-monsoon period. BrC AAOD is maximum (~0.02) over Kathmandu during the pre-monsoon period, and also remains high during the monsoon. This is consistent with the increase in the abundance of biomass burning aerosols over the Himalayas in these seasons, beyond the residential biomass burning emissions, which remain fairly constant throughout the year (Sadavarte et al., 2019). BrC AAOD at all other locations in the IGP (except over New Delhi in the winter) is lower than Kathmandu throughout the year except during the post-monsoon season (Fig. 7d). BC

Table 3
Annual mean aerosol optical depth (AOD) – total, black carbon (BC) and brown carbon (BrC), single scattering albedo (SSA), absorption AOD (AAOD), percentage contribution of carbonaceous aerosol (CA) and dust to AAOD, and percentage contribution of black carbon (BC) and brown carbon (BrC) to carbonaceous aerosol (CA) AAOD corresponding to a wavelength of 550 nm, along with ± 1σ (standard deviation) for AOD (total, BC and BrC), SSA and AAOD over the study locations (rounded off to 2 decimal digits).

Location	AOD			SSA	AAOD	%Contribution		%Contribution	
	Total	BC	BrC			CA	Dust	BC	BrC
Lumbini	0.59 ± 0.13	0.04 ± 0.02	0.04 ± 0.03	0.93 ± 0.03	0.04 ± 0.03	96	4	88	12
Pokhara	0.40 ± 0.19	0.04 ± 0.02	0.06 ± 0.03	0.91 ± 0.02	0.05 ± 0.02	87	13	81	19
Kathmandu	0.34 ± 0.16	0.07 ± 0.03	0.07 ± 0.04	0.87 ± 0.03	0.07 ± 0.03	98	2	85	15
Karachi	0.48 ± 0.23	0.02 ± 0.01	0.03 ± 0.01	0.92 ± 0.02	0.04 ± 0.01	63	37	81	19
Lahore	0.57 ± 0.13	0.03 ± 0.01	0.04 ± 0.02	0.91 ± 0.02	0.06 ± 0.02	55	45	75	25
New Delhi	0.61 ± 0.12	0.06 ± 0.04	0.08 ± 0.06	0.87 ± 0.06	0.08 ± 0.04	82	18	82	18
Kanpur	0.70 ± 0.08	0.04 ± 0.02	0.05 ± 0.02	0.92 ± 0.01	0.05 ± 0.01	76	24	78	22
Gandhi College	0.72 ± 0.12	0.04 ± 0.01	0.05 ± 0.02	0.92 ± 0.02	0.05 ± 0.02	82	18	83	17
Dhaka	0.71 ± 0.15	0.06 ± 0.02	0.05 ± 0.03	0.91 ± 0.03	0.06 ± 0.03	94	6	88	12
Bhola	0.59 ± 0.12	0.05 ± 0.03	0.04 ± 0.02	0.92 ± 0.03	0.05 ± 0.02	98	2	87	13
East Asia*									
Gosan	0.35 ± 0.25			0.95 ± 0.03	0.021			85	15
Anmyon	0.38 ± 0.24			0.95 ± 0.02	0.023			85	15
Baengnyeong	0.34 ± 0.30			0.96 ± 0.02	0.015			84	16
Shirahama	0.23 ± 0.17			0.95 ± 0.03	0.019			89	11
Fukuoka	0.27 ± 0.19			0.95 ± 0.02	0.018			90	10
Seoul	0.44 ± 0.37			0.96 ± 0.02	0.023			93	7
Gwangju	0.41 ± 0.32			0.95 ± 0.02	0.023			93	7
Beijing	0.70 ± 0.52			0.93 ± 0.03	0.055			90	10
Xianghe	0.73 ± 0.53			0.94 ± 0.03	0.048			92	8
Xuzhou	0.73 ± 0.46			0.94 ± 0.03	0.031			93	7
Taihu	0.73 ± 0.49			0.94 ± 0.02	0.038			93	7
Hongkong	0.44 ± 0.30			0.93 ± 0.03	0.036			91	9
Chiba	0.17 ± 0.12			0.95 ± 0.02	0.016			92	8
Osaka	0.27 ± 0.20			0.95 ± 0.03	0.019			93	7

*East Asian results are taken from Cho et al. (2019). SSA corresponds to 675 nm wavelength.

contributes ≥ 80% to the AAOD throughout the year over the Himalayas, while it contributes ≥ 75% to AAOD over the IGP (Fig. 7e, f).

BC and BrC AODs are always greater than their respective AAOD values (Fig. 7a-d, Table 3) because of their SSA (BC SSA = 0.19, BrC SSA = 0.85), i.e. for the same AAOD, the AOD for BrC would be > 5-times as large as that of BC. The BrC AOD is more than the BC AOD over all the locations except Lumbini (equal), Dhaka and Bhola (Table 3) (BrC contributes < 15% to the annual mean AAOD in these locations). The AAODs due to dust, BC and BrC deduced over South Asia from observations in this study are significantly higher than previously published model estimates (Chung et al., 2012a). The empirical estimates of global average, annual-mean AODs are 0.0095, 0.0077 and 0.0018 for CA, BC and BrC (Chung et al., 2012a); the range due to parameter uncertainties and observational errors in the above estimates were reported to be 0.008 to 0.01, 0.006–0.009 and 0.001–0.003 for CA, BC and BrC respectively. The global average annual-mean dust AAOD is 0.00093 (Chung et al., 2012a). The AAODs due to dust, CA, BC, and BrC estimated in this study are at least higher by 25 to 50% during the year as compared to the above model estimates over this region, and the differences become even higher when compared to global annual average values. The multi-model mean of ACCMIP strongly underestimates AAOD (Shindell et al., 2013). The spatial correlations between model simulated AAOD and OMI retrieved AAOD were reportedly poor, and the models underestimate AAOD by a factor of 2 (Shindell et al., 2013).

The light-absorption due to BrC, which is effective over the wavelength region of 300 to 600 nm, peaks around 365–370 nm (near-UV regime), however, AERONET AAODs were available for the lowest wavelength at 440 nm. Therefore, we use the AAODs obtained at 440 nm, and derived the contribution due to CA, BC and BrC aerosols to AAOD at 440 nm (Fig. 8) following the same procedure adopted for 550 nm. At the outset, it is clear that the AAOD, and CA, BC and BrC AAODs at 440 nm are higher than at 550 nm confirming the effectiveness of BrC in light-absorption at wavelengths lower than 550 nm, however, the seasonal and spatial patterns are same between 550 (Fig. 7) and 440 nm (Fig. 8). AAE in the wavelength range of 440 to 675 nm for CA aerosols was derived using CA AAODs obtained at 440 and 675 nm. Since the AAE value for CA aerosols is the same for 440, and 550 nm the percentage contributions of BC and BrC to CA AAOD are also same, however, the absolute values of BC and BrC AAOD are higher at 440 nm (Fig. 8).

The annual mean AAOD at 550 nm is higher, and the SSA is lower over these South Asia sites (Table 3) than at several urban sites (Seoul, Gwangju, Beijing, Xianghe, Xuzhou, Taihu, Hongkong, Chiba and Osaka), and background sites (Gosan, Anmyon, Baengnyeong, Shirahama and Fukuoka) in East Asia (20-40°N, 110-140°E) (Cho et al., 2019). The annual mean contribution of BC to CA AAOD in East Asia (Cho et al., 2019), derived using the same approach (Chung et al., 2012a; Cho et al., 2019) was higher over urban stations (92 ± 4%) than background stations (87 ± 2%). In contrast, over South Asia the annual mean BC contribution varies from a low value of 75% (Lahore) to a high value of 88% (Lumbini and Dhaka, Table 3).

Over East Asia BrC has been found to contribute more to the AAOD due to CA at background sites (10–16%) (Table 3) than at urban, polluted sites (7–10%) (Cho et al., 2019). Information on dust AAOD and their percentage contributions were not provided in Cho et al. (2019). In comparison, over South Asia BrC contributes significantly more (12–25%) to the AAOD due to CA. The greater contribution of BrC to AAOD over South Asia reveals the dominant influence of biomass burning emissions in this region. Among the capital cities in South Asia considered in this study, and in East Asia considered in a previous study (Cho et al., 2019), the aerosol absorption is the highest over New Delhi, and correspondingly the SSA is the lowest. On an annual mean basis, dust contributes between 18 and 45% to the AAOD over South Asia, more especially at the dust-influenced locations (Table 3, Fig. 1), with Lahore and Karachi being the most influenced. The BrC AOD was found to be almost equal to the BC AOD (so that BrC contributed ~ 15% to the CA AAOD) over the background locations in East Asia, while it was

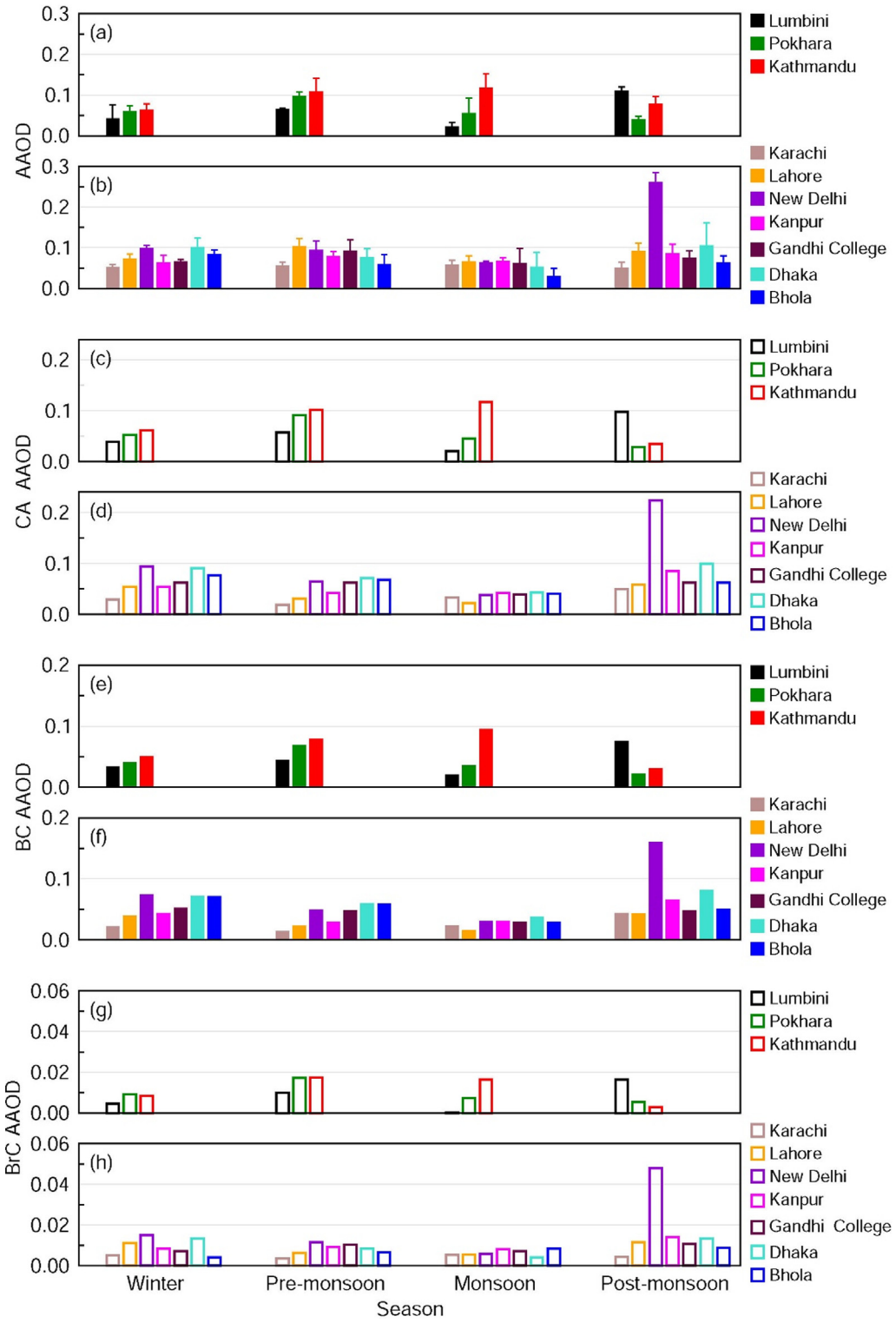

Fig. 8. Carbonaceous aerosol (CA), black carbon (BC) and brown carbon (BrC) over the IGP and the Himalayan Foothills: Seasonal mean values of (a, b) AAOD, (c, d) CA AAOD, (e, f) BC AAOD, and (g, h) BrC AAOD corresponding to a wavelength of 440 nm. Vertical bars in (a, b) represent ± 1σ standard deviation from the mean.

significantly lower than the BC AODs observed over the urban sites (Cho et al., 2019) (where BrC contributed ≤ 10% to the CA AAOD). In contrast, the AOD of BrC is always either equal or significantly higher (1.5-times) than that of BC over South Asia, reconfirming the dominant influence that biomass burning emissions have on the absorption characteristics of aerosols over South Asia.

Recent studies have clearly shown that the sites in the Himalayan foothills are heavily affected by regional emissions (it is true for the IGP sites as well); for example, Singh et al. (2019) attributed elevated layers of aerosols observed over the Pokhara Valley in the Himalayan foothills to regional emissions in the IGP and the Himalayan foothills; Mahapatra et al. (2019), using both in situ observations and model simulation with currently available regional emission inventory, found a significant part of AOD and $PM_{2.5}$ observed over the Kathmandu Valley

was due to regional emissions; and Lüthi et al. (2015) demonstrated transport of particulate matter from IGP to the remote part of the Tibetan Plateau across the Himalayas. Therefore, the local emission inventory of various aerosol species does not necessarily capture the columnar-aerosol characteristics especially in a region like the Himalayan-Tibetan Plateau mountain regions which are affected heavily by regional pollution. In order to apportion contributions of local and regional emissions of light-absorbing aerosols to the observed AODs over these sites new improved emission inventories (including BrC, which is not included in current inventories) would be needed, along with atmospheric simulations with regional chemistry transport models like the Weather Research and Forecasting (WRF) model coupled with Chemistry (WRF-Chem). Such emission inventories are just becoming available (such as for example, Nepal emission inventory by Sadavarte et al., (2019) which does not yet include BrC), and the required extensive model simulations will hopefully be the subject of follow-up studies. In addition, it should be noted that the aerial distances between Lumbini and the Pokhara Valley, and between the Pokhara Valley and the Kathmandu Valley are on the order of about 100 km. Thus, because of the regional homogeneity and influence, commonality in aerosol sources and emissions, and the nominal spatial distance between the locations, the conclusions drawn on light-absorption properties based on the observations at different altitudes at different locations in the same region can be deemed to be representative of the results obtained at different altitudes at a single site in this region. Moreover, it is difficult to compare BrC absorption from in situ observations on the surface with columnar BrC AAOD data because of the fact that the vertical changes in the BrC distribution are not generally known (Kirillova et al., 2016).

5. Implications and summary

An analysis of new and high quality in situ observations of columnar aerosol absorption over the Indo-Gangetic Plain (IGP) and the Himalayan foothills region, a relatively poorly studied region with several sensitive ecosystems of global importance, as well as highly vulnerable populations, reveals that the aerosol absorption over South Asia is higher than several urban and background sites in East Asia, and also higher than model estimates. Such high amounts of light-absorbing BC and BrC over the Himalayas have significant implications for the regional climate and hydrological cycle. On a regional scale, BC is the dominant absorbing aerosol type, but its dominance was found to vary across locations in South Asia (this study) and East Asia (Cho et al., 2019). The contribution of BrC to AAOD differs between South and East Asia. BC dominates over BrC for aerosol absorption over South Asia throughout the year, with both exhibiting strong seasonal and regional variations due to emission sources and transport. This analysis shows that over the IGP, the dust contribution to AAOD increases to ca. 30% during the pre-monsoon season due to transport from nearby arid and desert regions. A greater contribution of BrC to the aerosol absorption (12–25%) at the observation sites across South Asia confirms the dominant influence of biomass burning emissions on aerosol properties throughout the year.

The regional scale aerosol-induced atmospheric warming, and the deposition of light-absorbing carbonaceous aerosols on snow and ice, can accelerate glacier and snow melt (Barnett et al., 2005). The Hindukush-Himalayan-Tibetan Plateau region, which contains the largest ice mass outside the Antarctic and Arctic polar regions, has witnessed a pronounced retreat in the glaciers, which is expected to negatively affect the water supply in South and East Asia, with significant consequences for the regional hydrological cycle (Kang et al., 2019; Barnett et al., 2005). The knowledge about quantitative contributions and seasonal variations of carbonaceous aerosols (BC and BrC) and dust aerosols across the IGP and the Himalayas was hitherto unavailable. The results from this study can help guide further studies to improve models of this region, and to quantify the effects of these aerosol types individually as well as collectively on climate, on glacier and snow melting over the mountain regions, and on the monsoon circulation, and help to evaluate the likely effectiveness of proposed mitigation actions and solution pathways.

Acknowledgements

We thank the principal investigators of each AERONET site for their efforts in establishing and maintaining the AERONET sites (https://aeronet.gsfc.nasa.gov/) the data of which are used in the study. This study was conducted when SR was a Senior Fellow at IASS on a sabbatical from Physical Research Laboratory, India. He is currently an Affiliate Scholar of IASS. **Funding:** This study is supported by IASS which is funded by the German Federal Ministry for Education and Research (BMBF) and the Brandenburg State Ministry for Science, Research and Culture (MWFK). MR and MGL acknowledge Brent N. Holben from the NASA AERONET for providing two sets of CIMEL Sunphotometers for setting up AERONET sites at Bode (Kathmandu Valley) and Lumbini. **Author Contributions:** MR set up and maintained the AERONET sites at Kathmandu and Lumbini. SR designed the study in consultation with MR and MGL. SR performed the analysis and wrote the paper. All authors reviewed and edited the paper. **Competing financial interests:** The authors declare no conflict of interests. **Data availability:** All the data used in the manuscript are publicly available at https://aeronet.gsfc.nasa.gov/.

Appendix A. Supplementary material

Supplementary data to this article can be found online at https://doi.org/10.1016/j.envint.2020.105814.

References

Barnett, T.P., Adam, J.C., Lettenmaier, D.P., 2005. Potential impact of a warming climate on water availability in snow-dominated regions. Nature 438, 303–309.
Bergstrom, R.W., et al., 2007. Spectral absorption properties of atmospheric aerosols. Atmos. Chem. Phys. 7, 5937–5943.
Cho, C., et al., 2017. Wintertime aerosol optical and radiative properties in the Kathmandu Valley during the SusKat-ABC field campaign. Atmos. Chem. Phys. 17, 12617–12632.
Cho, C., et al., 2019. Observation-based estimates of the mass absorption cross-section of black and brown carbon and their contribution to aerosol light absorption in East Asia. Atmos. Env. 212, 65–74.
Chung, C.E., Ramanathan, V., Decremer, D., 2012a. Observationally constrained estimates of carbonaceous aerosol radiative forcing. PNAS 109, 11624–11629.
Chung, C.E., Lee, K., Müller, D., 2012b. Effect of internal mixture on black carbon radiative forcing. Tellus B 64, 10925.
Dubovik, O., Smirnov, A., Holben, B.N., King, M.D., Kaufman, Y.J., Eck, T.F., Schuster, I., 2000. Accuracy assessments of aerosol optical properties retrieved from Aerosol Robotic Network (AERONET) Sun and Sky radiance measurements. J. Geophys. Res. 105, 9791–9806.
Eck, T.F., et al., 2010. Climatological aspects of the optical properties of fine/coarse mode aerosol mixtures. J. Geophys. Res. 115, D19205. https://doi.org/10.1029/2010JD014002.
Gustafsson, Ö., et al., 2009. Brown clouds over South Asia: Biomass or fossil fuel combustion. Science 323, 495–498.
Holben, B.N., et al., 2001. An emerging ground-based aerosol climatology: Aerosol optical depth from AERONET. J. Geophys. Res. 106, 12067–12097.
IPCC, 2013. Summary for Policymakers. In: Stocker, T.F., Qin, D., Plattner, G.-K., Tignor, M., Allen, S.K., Boschung, J., Nauels, A., Xia, Y., Bex, V., Midgley, P.M. (Eds.), Climate Change 2013: The Physical Science Basis. Contribution of Working Group I to the Fifth Assessment Report of the Intergovernmental Panel on Climate Change. Cambridge University Press, Cambridge, United Kingdom and New York, NY, USA, 1-28 pp.
Jethva, H., Chand, D., Torres, O., Gupta, P., Lyapustin, A., Patadia, F., 2018. Agricultural burning and air quality over northern India: A synergistic analysis using NASA's A-train satellite data and ground measurements. AAQR 18, 1756–1773.
Jimenez, J.L., et al., 2009. Evolution of organic aerosols in the atmosphere. Science 326, 1525.
Kang, S.K., et al., 2019. Linking atmospheric pollution to cryospheric change in the Third Pole region: current progress and future prospects. Nat. Sci. Rev. 6. https://doi.org/10.1093/nsr/nwz031.
Kirchstetter, T.W., Novakov, T., Hobbs, P.V., 2004. Evidence that the spectral dependence of light absorption by aerosols is affected by organic carbon. J. Geophys. Res. 109, D21208. https://doi.org/10.1029/2004JD004999.

Kirillova, E.N., Marinoni, A., Bonasoni, P., Vuillermoz, E., Facchini, M.C., Fuzzi, S., Decesari, S., 2016. Light absorption properties of brown carbon in the high Himalayas. J. Geophys. Res. 121, 9621–9639. https://doi.org/10.1002/2016JD025030.

Lawrence, M.G., Lelieveld, J., 2010. Atmospheric pollutant outflow from southern Asia: a review. Atmos. Chem. Phys. 10, 11017–11096.

Li, C., et al., 2016. Sources of black carbon to the Himalayan-Tibetan Plateau glaciers. Nat. Comm. 7, 12574. https://doi.org/10.1038/ncomms12574.

Lüthi, Z.L., Skerlak, B., Kim, S.W., Lauer, A., Mues, A., Rupakheti, M., Kang, S.C., 2015. Atmospheric brown clouds reach the Tibetan Plateau by crossing the Himalayas. Atmos. Chem. Phys. 15, 6007–6021.

Magi, B.I., 2011. Chemical apportionment of southern African aerosol mass and optical depth - Corrigendum. Atmos. Chem. Phys. 11, 4777–4778.

Mahapatra, P.S., Puppala, P.S., Adhikary, B., Shrestha, K.L., Dawadi, D.P., Paudel, S.P., Panday, A., 2019. Air quality trends of the Kathmandu Valley: A satellite, observation and modeling perspective. Atmos. Env. 201, 334–347.

Mallet, M., et al., 2013. Absorption properties of Mediterranean aerosols obtained from multi-year ground-based remote sensing observations. Atmos. Chem. Phys. 13, 9195–9210.

Maurer, J.M., Schaefer, J.M., Rupper, S., Corely, A., 2019. Acceleration of ice loss across the Himalayas over the past 40 years. Sci. Adv. 5, eaav7266.

Menon, S., et al., 2010. Black carbon aerosols and the third polar ice cap. Atmos. Chem. Phys. 10, 4559–4571.

Ramachandran, S., Kedia, S., Sheel, V., 2015. Spatiotemporal characteristics of aerosols in India: Observations and model simulations. Atmos. Env. 116, 225–244.

Ramanathan, V., et al., 2007. Atmospheric brown clouds: Hemispherical and regional variations in long-range transport, absorption, and radiative forcing. J. Geophys. Res. 112. https://doi.org/10.1029/2006JD008124.

Russell, P.B., et al., 2010. Absorption Ångström Exponent in AERONET and related data as an indicator of aerosol absorption. Atmos. Chem. Phys. 10, 1155–1169.

Sadavarte, P., Rupakheti, M., Bhave, P., Shakya, K., Lawrence, M., 2019. Nepal Emission Inventory – Part I: Technologies and combustion sources (NEEMI-Tech) for 2001–2016. Atmos. Chem. Phys. 19, 12953–12973.

Sato, M., et al., 2003. Global atmospheric black carbon inferred from AERONET. PNAS 100, 6319–6324.

Shindell, D.T., et al., 2013. Radiative forcing in the ACCMIP historical and future climate simulations. Atmos. Chem. Phys. 13, 2939–2974.

Singh, A., Mahata, K.S., Rupakheti, M., Junkermann, W., Panday, A.K., Lawrence, M.G., 2019. An overview of airborne measurement in Nepal – Part 1: Vertical profile of aerosol size, number, spectral absorption, and meteorology. Atmos. Chem. Phys. 9, 245–258.

Textor, C., et al., 2006. Analysis and quantification of the diversities of aerosol life cycles within AeroCom. Atmos. Chem. Phys. 6, 1777–1813.

Weissmann, M., Braun, A.F.J., Gantner, A.L., Mayr, A.G.J., Rahm, A.S., Reitebach, A.O., 2005. The Alpine Mountain-Plain circulation: airborne Doppler Lidar measurements and numerical calculations. Mon. Weather Rev. 133, 3095–3109.

Xu, Y., Ramanathan, V., Washington, W.M., 2016. Observed high-altitude warming and snow cover retreat over Tibet and the Himalayas enhanced by black carbon aerosols. Atmos. Chem. Phys. 16, 1303–1315.